Research in Astron. Astrophys. **2010** Vol. **10** No. **12**, 1265–1274
http://www.raa-journal.org *http://www.iop.org/journals/raa*

***R**esearch in*
***A**stronomy and*
***A**strophysics*

Asteroseismic study of the red giant ϵ Ophiuchi *

Shao-Lan Bi[1], Ling-Huai Li[2], Yan-Ke Tang[3] and Ning Gai[1]

[1] Department of Astronomy, Beijing Normal University, Beijing 100875, China; *bisl@bnu.edu.cn*
[2] Department of Astronomy, Yale University, P.O. Box 208101, New Haven, CT 06520-8101, USA
[3] Department of Physics, Dezhou University, Dezhou 253023, China

Received 2010 June 8; accepted 2010 July 27

Abstract We test the possible evolutionary tracks of stars with various masses $(1.8\,M_\odot, 1.9\,M_\odot, 2.0\,M_\odot, 2.1\,M_\odot, 2.2\,M_\odot)$ and metallicities Z (0.008, 0.010, 0.012), including both models with and without convective core overshooting. At a given mass and metallicity, the models with a larger overshoot predict a larger radius and age of the star. Based on the observed frequency of oscillations and the position of ϵ Oph on the H-R diagram, we obtain two distinct better-fitting models: the solutions with mass $M = 1.9\,M_\odot$ favor a radius in the range $10.55 \pm 0.03\,R_\odot$ with an age of 1.01 ± 0.08 Gyr; the solutions with mass $M = 2.0\,M_\odot$ favor a radius in the range $10.74 \pm 0.03\,R_\odot$ with an age of 0.95 ± 0.11 Gyr. Furthermore, we investigate the influence of overshooting on the internal structure and the pulsation properties, and find that increasing the convective core overshoot significantly decreases non-radial mode inertia, while also increasing the mode amplitude. Therefore, the estimation of stellar mass and age might be modified by convective core penetration.

Key words: stars: oscillations — stars: individual: ϵ Ophiuchi — stars: interiors

1 INTRODUCTION

Observations based on ground and space missions have shown that solar-like oscillations can be excited stochastically by convection in several G and K-class red giant stars (Frandsen et al. 2002; De Ridder et al. 2006, 2009; Barban et al. 2007; Hekker et al. 2009; Kallinger et al. 2008, 2009). These stars are very different from main sequence stars, with a highly condensed core, and low density envelope. Therefore, red giant stars are extremely difficult to model since they can be in very different states of evolution, and still be at the same place on the HR-diagram, which makes it difficult to determine their stellar parameters.

The G9.5 giant star ϵ Oph (HD 146791, HR 6075) has been well-determined in terms of its parallax and atmosphere parameters. The basic stellar parameters are summarized in Table 1. This will allow us to locate the star on the H-R diagram. Recently, the asteroseismic analysis of the red giant ϵ Oph using space- and ground-based data (De Ridder et al. 2006; Hekker et al. 2006; Barban et al. 2007; Kallinger et al. 2008) has reliably identified the presence of radial and non-radial oscillation modes, characterized by a possible mean value of the large separation of $5.3 \pm 0.1\,\mu$Hz and frequencies in the range $25 - 80\,\mu$Hz. The discovery of solar-like oscillations in the

* Supported by the National Natural Science Foundation of China.

red giant star ϵ Oph opened up a new part of the Hertzsprung-Russell diagram to be explored with asteroseismic techniques.

Table 1 Observational Constraints

Parameters	ϵ Oph	References
$T_{\rm eff}$ (K)	4877 ± 100	De Ridder et al. (2006)
$L/L_\odot$	59 ± 5	De Ridder et al. (2006)
$R/R_\odot$	10.4 ± 0.45	Richichi et al. (2005)
[Fe/H]	–0.25	Cayrel de Strobel et al. (2001)
$\Delta\nu_0$ (μHz)	5.3 ± 0.1	Barban et al. (2007)

It has already been demonstrated that both the shell H-burning models and the core He-burning models with a mass of about $2.0\,M_\odot$ successfully account for most of the observed properties of ϵ Oph (De Ridder et al. 2006; Kallinger et al. 2008; Mazumdar et al. 2009). However, a more detailed description of possible models, including core overshooting during the central hydrogen-burning phase, should be considered. Since ϵ Oph has a deep convective envelope and a very small core, where the low-degree p-modes penetrate, the oscillation frequencies are sensitive to the mass of the helium core and the composition profile of the central regions, and hence to the age of the star and the presence and extent of overshoot (Audard et al. 1995; Di Mauro et al. 2003; Bi et al. 2008).

In this paper, we mainly investigate the effects of the overshooting on the models and properties of oscillations of ϵ Oph based on the observational constraints. In Section 2, for various masses and metallicities, we construct a grid of stellar models which are characterized by non-asteroseismic and asteroseismic observational constraints. In addition, we illustrate the characteristics of models with and without overshooting. In Section 3, we analyze the properties of oscillations of low-degree p-modes, and show the sensitivity of the frequencies of oscillation on the core overshooting. In Section 4, we discuss our results.

2 MODELS

2.1 Stellar Models

Stellar evolutionary models were constructed with the Yale Rotating Stellar Evolution Code (YREC; Guenther et al.1992). The initial zero-age main sequence (ZAMS) model was calculated from pre-main sequence evolution. The post-main sequence models of various compositions were then constructed by first rescaling the composition of ZAMS models. In the computation, we used updated OPAL equation of state tables EOS2005 (Rogers & Nayfonov 2002), the opacities were a smooth blend of OPAL GN93 (Iglesias & Rogers 1996) and the low temperature tables GS98ferg (Ferguson et al. 2005), and we implemented the mixing-length theory for convection. Here diffusion, rotation and magnetic fields were neglected. Our main goal is to show the importance of the influence of overshooting on the stellar interior structure, as well as on the radial and non-radial stellar oscillations. The overshoot produces a chemical mixing in the region where the turbulent motions penetrate from the edge of the convective core to a radial extent $l_{\rm ov}$ defined by a parameter $\alpha_{\rm ov}$: $l_{\rm ov} = \alpha_{\rm ov}\min(r_{\rm c}, H_{\rm p})$, where $H_{\rm p}$ is the pressure scale height at the edge of the core, $r_{\rm c}$ is the radius of the convective core and $\alpha_{\rm ov}$ is a non-dimensional parameter typically below unity. The above expression is used to limit the extent of the overshoot region to be no larger than a fraction $\alpha_{\rm ov}$ of the size of the core.

In order to investigate the dependence of our models on the input physics used, we calculated the evolutionary tracks with different input parameters for masses $M = (1.8\,M_\odot, 1.9\,M_\odot, 2.0\,M_\odot, 2.1\,M_\odot, 2.2\,M_\odot)$, metal abundances $Z = (0.008, 0.010, 0.012)$ and overshoot parameters $\alpha_{\rm ov} = (0.0, 0.1, 0.2, 0.3, 0.4, 0.5, 0.6)$, by using a mixing-length parameter $\alpha = 1.75$ and an initial

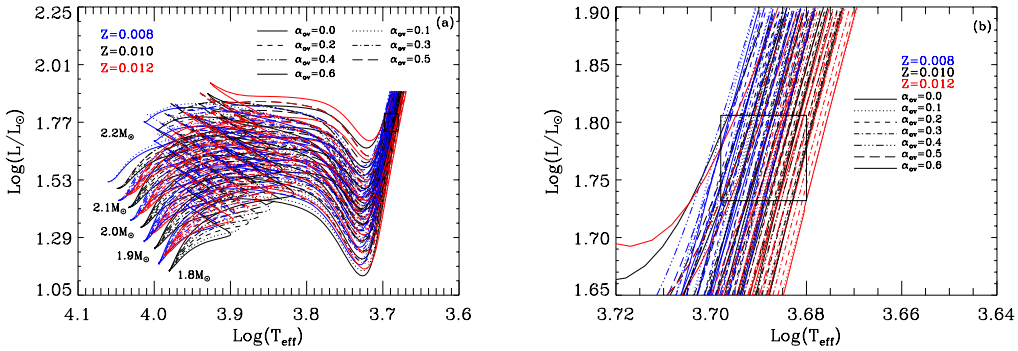

Fig. 1 (a) Evolutionary tracks of ϵ Oph in the H-R diagram from the ZAMS to the shell H-burning RGB, calculated for a range of stellar models of masses $M = (1.8\,M_\odot, 1.9\,M_\odot, 2.0\,M_\odot, 2.1\,M_\odot, 2.2\,M_\odot)$, metal abundances $Z = (0.008, 0.010, 0.012)$ and overshooting parameters $\alpha_{\rm ov} = (0.0, 0.1, 0.2, 0.3, 0.4, 0.5, 0.6)$, to match the observed error box. The error box indicates the observational constraints of $L/L_\odot$ and $T_{\rm eff}$; (b) The zoomed in part of the error box.

helium abundance $Y = 0.275$ calibrated with a solar model. It is noted that we adopted the new solar abundance $[Z/X]_\odot = 0.0178$ (Asplund et. al 2005; Cunha et al. 2006) in converting [Fe/H] to Z values. Figure 1 displays the computed evolutionary tracks which are characterized by the observed $(T_{\rm eff}, L/L_\odot)$ within the error box in the H-R diagram. In addition, we also calculated the evolutionary tracks with overshooting parameter $\alpha_{\rm ov} > 0.6$. These models are not able to reproduce the observational constraints, especially in the observed radius of the star in $\pm 1\sigma$.

Comparing the evolutionary tracks with and without overshooting in Figure 1, by varying the overshoot parameter $\alpha_{\rm ov}$ from 0.0 to 0.6, we find that the location of the star in the HR diagram sensitively depends on the extent of the overshoot parameter $\alpha_{\rm ov}$. At a fixed effective temperature, a model with a larger overshoot distance is more luminous and more evolved than a model with less overshoot. The most important hint is that overshooting produces an extension of the mixed core during the main-sequence phase, hence the model with a core overshoot exhibits the property that the central hydrogen content is larger than the model without overshooting. As a result, the time spent on the main sequence increases, and the turn-off point, where nearly all the hydrogen is burnt in the core, occurs at a smaller effective temperature. This property indicates that there is a very strong correlation between stellar luminosity and the mass of the helium core along the RGB.

In addition, Figure 1 shows that the evolutionary track moves down toward the right side of the H-R diagram with increasing metal abundance Z for a giving mass. This may be because the ionization temperatures of metals are low, hence an increased Z will produce more electrons in the surface layer, resulting in more negative hydrogen ions H^- being formed. An increase of opacity due to the increase in hydrogen abundance leads to a decrease of the effective temperature and luminosity. Therefore, the position at the base of the red-giant branch of ϵ Oph with higher metal abundance Z is lower than the one with lower Z in the H-R diagram. The star with a higher Z is less evolved than one with a lower Z.

2.2 Model Calibration

We calculated eigenfrequencies with low-degree p-modes $\ell = 0 - 3$ for all the selected structure models, which fall into the observed $(T_{\rm eff}, L/L_\odot)$ error box, by using Guenther's stellar pulsation code (Guenther 1994). The theoretical oscillation spectrum, which uses the selected models of ϵ

Oph, is characterized by acoustic modes with frequencies in the range $\sim 10 - 100\,\mu$Hz from radial order $n = 1$ to the acoustic cutoff frequency.

In seismic analysis, the frequencies $\nu_{n,\ell}$ of oscillation modes, characterized by the radial order n at harmonic degree ℓ, satisfy a simple asymptotic relation (Tassoul 1980)

$$\nu_{n,\ell} \sim \Delta\nu \left(n + \frac{\ell}{2} + \epsilon \right), \tag{1}$$

where $\Delta\nu = \left(2\int_0^R dr/c\right)^{-1}$ is the inverse of the sound travel time across a stellar diameter, and ϵ is a function of frequency that depends mainly on the conditions near the surface region. The asteroseismic features, i.e. the large spacings $\Delta\nu$, are a very useful tool to provide the comparison between models and observations, defined by

$$\Delta\nu_{n,\ell} \equiv \nu\,(n,\ell) - \nu\,(n-1,\ell)\,. \tag{2}$$

Once the value of the mean large spacing is determined for each model of ϵ Oph by taking the average of the theoretical separations, we can use χ^2_C minimization to deduce the best agreement with the observations. Furthermore, following the work done by Kallinger et al. (2008) for the analysis of p-mode frequencies in ϵ Oph, we also carried out an additional χ^2_νcomparison between theoretical and observed frequencies. Therefore, for each comparison, we computed the values of the following functions, defined as:

$$\chi^2_C = \sum_{i=1}^{5} \left(\frac{C_i^{\rm theo} - C_i^{\rm obs}}{\delta C_i^{\rm obs}} \right)^2, \tag{3}$$

$$\chi^2_\nu = \frac{1}{N} \sum_{i=1}^{N} \left(\frac{\nu_i^{\rm theo} - \nu_i^{\rm obs}}{\delta \nu_i^{\rm obs}} \right)^2, \tag{4}$$

where the vector $\mathbf{C} \equiv (T_{\rm eff}, L/L_\odot, R/R_\odot,$ [Fe/H], $\Delta\nu_0)$ and frequency ν represent the observational and theoretical values of the star, respectively, δ is the corresponding observational errors, which are given in Table 1, and $N = 9$ is the total number of radial order modes (Barban et al. 2007).

For a grid of models of 89 evolutionary tracks which fall within the observational error box, we calculated all values of χ^2_C and χ^2_ν. Among the selected models, we found that the lowest value of χ^2_C reasonably matches χ^2_ν minimization, so we choose the model with $\chi^2_\nu \leq 10$ as the better fitting model. Table 2 lists the characteristics of 33 candidates by searching for minima in χ^2_C and χ^2_ν: metallicity, overshoot parameter, effective temperature, luminosity, radius, age and so on.

Figure 2 shows the location of the 33 best-fitting models in the H-R diagram, delimited by the observed radius in $\pm 1\sigma$. As expected, significant differences appear between the positions of overshooting models for fixed values of mass and metallicity. According to the observational constraints, with all the possible values of mass, metallicity and overshooting, we obtain two better-fitting models: the mass $M = 1.9\,M_\odot$ favors a radius in the range of $10.55 \pm 0.03\,R_\odot$ with an age of 1.01 ± 0.08 Gyr; the mass $M = 2.0\,M_\odot$ favors a radius in the range of $10.74 \pm 0.03\,R_\odot$ with an age of 0.95 ± 0.11 Gyr. Despite the positions of models with various overshoot parameters $\alpha_{\rm ov}$ being very near to each other in the HR-diagram for given mass and metallicity values, the depth of the convection zone decreases with the increase in the overshoot parameter $\alpha_{\rm ov}$. Furthermore, the result identifies ϵ Oph as being in the ascending phase on the red-giant branch corresponding to the shell H-burning phase of evolution. It is evident that the characteristics of the models and the oscillation frequencies depend significantly on the value of $\alpha_{\rm ov}$. The following analysis is expected to reveal the presence of overshooting and its effect on the associated stellar properties.

Table 2 Model Parameters by χ^2_C and χ^2_ν Minimization

Star	$M/M_\odot$	X	Z	$\alpha_{\rm ov}$	$\log T/T_{\rm eff}$	$\log L/L_\odot$	$R/R_\odot$	$r_{\rm cz}/R_\odot$	Age (Gyr)	$\Delta\nu_0$	χ^2_C	χ^2_ν
1	1.8	0.717	0.008	0.0	3.6884	1.7365	10.36	0.908	1.040	5.39	0.41	4.11
2	1.8	0.717	0.008	0.2	3.6885	1.7407	10.39	1.806	1.086	5.38	0.33	4.69
3	1.9	0.717	0.008	0.0	3.6902	1.7570	10.50	1.001	0.866	5.40	0.32	5.90
4	1.9	0.717	0.008	0.1	3.6903	1.7591	10.53	1.113	0.887	5.38	0.22	3.66
5	1.9	0.717	0.008	0.2	3.6908	1.7622	10.54	1.271	0.928	5.38	0.49	4.31
6	1.9	0.717	0.008	0.3	3.6915	1.7668	10.56	1.510	0.975	5.38	0.24	3.84
7	1.9	0.717	0.008	0.4	3.6923	1.7713	10.58	1.834	1.027	5.38	0.26	3.55
8	1.9	0.717	0.008	0.5	3.6934	1.7773	10.60	2.246	1.077	5.39	0.26	3.90
9	1.9	0.715	0.010	0.0	3.6855	1.7380	10.53	0.968	0.927	5.39	0.41	3.93
10	1.9	0.715	0.010	0.1	3.6858	1.7401	10.52	1.039	0.945	5.38	0.36	3.79
11	1.9	0.715	0.010	0.2	3.6861	1.7437	10.54	1.199	0.990	5.38	0.33	3.84
12	1.9	0.715	0.010	0.3	3.6868	1.7473	10.55	1.402	1.040	5.38	0.29	3.83
13	1.9	0.715	0.010	0.4	3.6876	1.7523	10.58	1.681	1.094	5.38	0.26	3.74
14	1.9	0.713	0.012	0.4	3.6828	1.7331	10.57	1.590	1.164	5.38	0.54	3.73
15	1.9	0.713	0.012	0.5	3.6836	1.7353	10.56	1.912	1.221	5.40	0.60	7.01
16	2.0	0.717	0.008	0.0	3.6918	1.7810	10.72	1.069	0.740	5.38	0.35	4.73
17	2.0	0.717	0.008	0.1	3.6922	1.7823	10.72	1.166	0.764	5.39	0.41	4.34
18	2.0	0.717	0.008	0.2	3.6928	1.7859	10.73	1.350	0.803	5.37	0.36	4.19
19	2.0	0.717	0.008	0.3	3.6936	1.7897	10.74	1.636	0.844	5.39	0.51	4.55
20	2.0	0.717	0.008	0.4	3.6945	1.7972	10.79	2.022	0.888	5.37	0.57	3.85
21	2.0	0.717	0.008	0.5	3.6958	1.8040	10.80	2.574	0.933	5.39	0.81	3.81
22	2.0	0.715	0.010	0.0	3.6872	1.7623	10.70	0.998	0.788	5.36	0.22	3.89
23	2.0	0.715	0.010	0.1	3.6876	1.7628	10.72	1.085	0.813	5.41	0.44	7.08
24	2.0	0.715	0.010	0.2	3.6882	1.7672	10.73	1.247	0.854	5.39	0.34	4.26
25	2.0	0.715	0.010	0.3	3.6888	1.7735	10.77	1.475	0.900	5.36	0.26	7.29
26	2.0	0.715	0.010	0.4	3.6898	1.7769	10.78	1.837	0.947	5.39	0.38	4.14
27	2.0	0.715	0.010	0.5	3.6910	1.7836	10.79	2.285	0.994	5.39	0.45	4.31
28	2.0	0.713	0.012	0.0	3.6825	1.7428	10.71	0.929	0.836	5.39	0.56	4.70
29	2.0	0.713	0.012	0.1	3.6828	1.7454	10.72	0.990	0.863	5.37	0.45	4.78
30	2.0	0.713	0.012	0.2	3.6835	1.7474	10.72	1.141	0.906	5.39	0.49	4.77
31	2.0	0.713	0.012	0.3	3.6841	1.7530	10.75	1.341	0.955	5.38	0.42	3.95
32	2.0	0.713	0.012	0.4	3.6850	1.7575	10.77	1.636	1.005	5.38	0.41	4.04
33	2.0	0.713	0.012	0.5	3.6862	1.7623	10.78	2.065	1.055	5.40	0.45	6.85

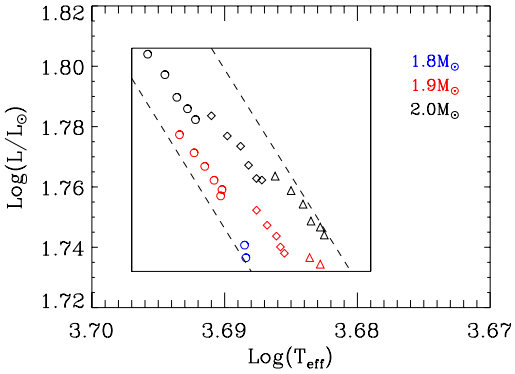

Fig. 2 Location of ϵ Oph in the H-R diagram for the 33 best-fitting models listed in Table 2. The dashed lines denote the error-box delimited by the observed radii. Open circles are used for $Z = 0.008$, diamonds for $Z = 0.010$ and triangles for $Z = 0.012$.

3 RESULTS

3.1 Effects on the Structure

For the evolved star ϵ Oph, the effects of convective core overshoot on the internal structure are directly reflected in the different chemical composition profiles near the helium core and at the base of the outer convective envelope, as shown in Figure 3. The flat portion of the curve indicates the convective envelope which is fully mixed. From Figure 3(c), we see that the hydrogen and helium abundances near the inner core are hardly affected by the various metallicity values, however they are sensitive to overshooting. It is clear that the central helium content increases with the increase of the overshoot parameter $\alpha_{\rm ov}$. Indeed, as the star evolves, the larger overshooting produces a larger extension of the mixed core during the main-sequence phase. In fact, the difference in the chemical composition profile due to overshooting affects the presence of the discontinuity in the gradient of the sound velocity and the steep peak in the Brunt-Väisälä frequency. Therefore, they give rise to strong constraints on the effects of overshooting on the internal structure.

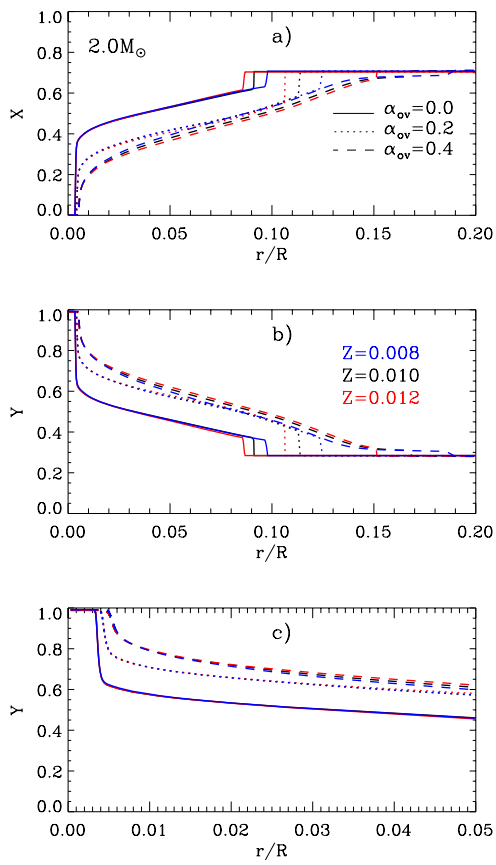

Fig. 3 Behavior of the hydrogen and helium abundance profiles in the central parts of $2.0\,M_{\odot}$ models M16, M18, M20, M22, M24, M26, M28, M30 and M32, computed without overshooting and including convective penetration from the core over 0.2 and 0.4 pressure scale heights.

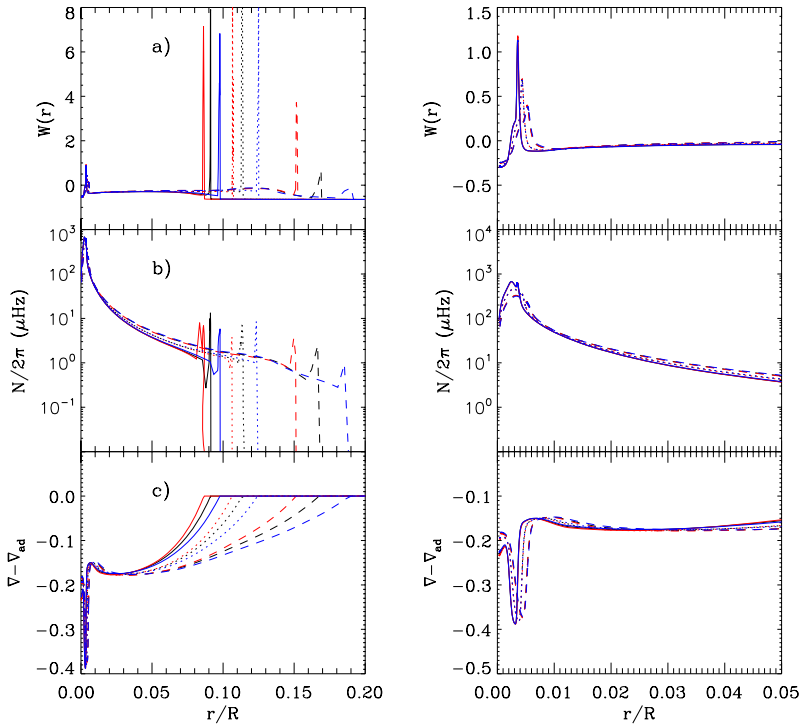

Fig. 4 Effects of convective-core overshooting on the internal structure of ϵ Oph. (a) Dimensionless gradient of sound speed, W(r), plotted as a function of radius. (b) The Brunt-Väisälä frequencies, $N/2\pi$, in the shell hydrogen-burning phase. (c) The super-adiabatic temperature gradient, $\nabla - \nabla_{\rm ad}$, as a function of radius. The same models and same line styles as in Fig. 3 are used.

Since sound speed increases very rapidly with depth, the variation may not be detectable in the sound-speed profile itself (Gough 1984; Basu & Antia 2008). The dimensionless gradient of the sound speed defined by

$$W(r) = \frac{1}{g}\frac{dc^2}{dr}, \tag{5}$$

sensitively depends on this variation, where g is the gravitational acceleration. Figure 4(a) illustrates that the behavior of the dimensionless sound speed was strongly affected by the variation of the chemical composition. Comparing Figures 3 and 4(a), we find that the rapid enhancement of the hydrogen abundance at the edge of the inner core and at the bottom of the convective envelope, respectively, cause abrupt changes in the dimensionless sound speed. As seen clearly in Figure 4(a), there are the shifts of prominent peaks in $W(r)$ corresponding to the contribution of variation of chemical composition due to the inclusion of various overshooting and metallicity attributes.

Like in Figure 4(a), the changing chemical composition also directly leads to a variation in the sharp feature in the Brunt-Väisälä frequency N^2, defined as (Unno et al. 1989; Christensen-Dalsgaard 2004)

$$N^2 = g\Big(\frac{1}{\Gamma_1}\frac{d\ln P}{dr} - \frac{d\ln\rho}{dr}\Big) \simeq \frac{g^2\rho}{P}(\nabla_{\rm ad} - \nabla + \nabla_\mu), \tag{6}$$

where $\nabla_{\rm ad} - \nabla$ is the superadiabatic gradient, and $\nabla_\mu = d\ln\mu/d\ln P$ is the gradient of the mean molecular weight μ. Figure 4(b) shows the behavior of the Brunt-Väisälä frequency with various overshoot parameters, in units of $\omega = \sqrt{GM/R^3}$, as a function of radius. It is only represented in

the radiative zones, since N^2 is negative in the convective zones. In the local mixing length theory, the boundary of the convective zone was defined by the Schwarzschild or Ledoux criterion: $\nabla > \nabla_{\rm ad}$ is convectively unstable, while $\nabla < \nabla_{\rm ad}$ is stable (radiative). From Figure 4(b), it is clear that if the boundary is defined as such, the star has a deep convective envelope. In addition, the position of the boundary of the convective zone has shifted outwards in radius and depends significantly on the value of the overshoot parameter. The depth of the convective envelope is reduced with increasing convective core overshoot.

The borders of the convective zone depend on the regions of rapid variation in the sound-speed gradient and Brunt-Väisälä frequency, due to a discontinuity in the super-adiabatic temperature gradient. This may result in changes in the stellar internal structure, and hence, this feature affects the oscillation frequencies. If the frequency precision is sufficiently high, the effects on frequencies of low-degree modes will be detectable. It can be used to put limits on the extent of overshoot beneath the convective envelope.

3.2 Mode Trapping

There are important differences in the oscillation properties between radial and non-radial modes. This difference is mainly reflected in a very useful characteristic of a mode, e.g. the value of its inertia, defined by (Christensen-Dalsgaard 2004)

$$E_{n\ell} \equiv \frac{M_{\rm mode}}{M} \equiv \frac{\int_V \rho |\delta \mathbf{r}| dV}{M |\delta \mathbf{r}|^2_{\rm ph}}, \tag{7}$$

where $\delta \mathbf{r}$ is the displacement eigenfunction, and the integration is over the volume of the star. For the simplest analysis of solar-like oscillations, the behavior of the inertia is also relevant for the amplitude of the modes. The expression of amplitude can be calculated by using an approximation

$$\frac{A_{n\ell}}{A_0(\nu)} \simeq \left[\frac{E_{n\ell}}{E_0(\nu)}\right]^{-1/2} \sim M_{\rm mode}^{-1/2}, \tag{8}$$

where A_0 and E_0 are the interpolation results of frequency for radial modes.

By analyzing the eigenfunctions of radial and non-radial modes, we see that the difference between radial and non-radial modes is mainly due to the mode inertia. Dupret et al. (2009) performed an interesting analysis of amplitude and mode inertia in the different evolutionary tracks of red giants. Here, we will analyze the important influence of overshooting on the radial and non-radial stellar oscillations. Figure 5(a) shows the behavior of the normalized mode inertia as a function of frequency for $1.9\,M_\odot$ models, i.e. M9 and M13 with overshooting parameters $\alpha_{\rm ov} = 0.0, 0.4$, respectively. For radial modes, the value of inertia decreases with increasing frequency. In the comparison of M9 and M13, there are no substantial differences between the cases with and without overshooting. The radial mode displays a purely acoustic characteristic, and follows an asymptotic behavior.

On the other hand, for the non-radial modes, we see that the inertia is very different and strongly depends on the strength of the overshooting parameters. There are a large number of modes which are dominated by a g-mode behavior and which show very high inertia. Moreover, for all cases with or without overshooting, the $\ell = 1$ modes, in which the surface inertia is higher than the radial mode inertia, maintain a mixed character. Hence, the mode trapped in the envelope is not perfect. This property indicates that p-mode and g-mode regions are not very strongly separated. These modes are strongly trapped in the interior. In addition, we have also found that increasing the core overshooting decreases the inertia for $\ell = 1$ modes by a factor of one. In contrast, we notice that a number of modes where $\ell = 2, 3$, for which the surface inertia is close to that of radial modes, behave as solar-like p modes. These modes are trapped mainly in the outer envelope. By including core overshooting,

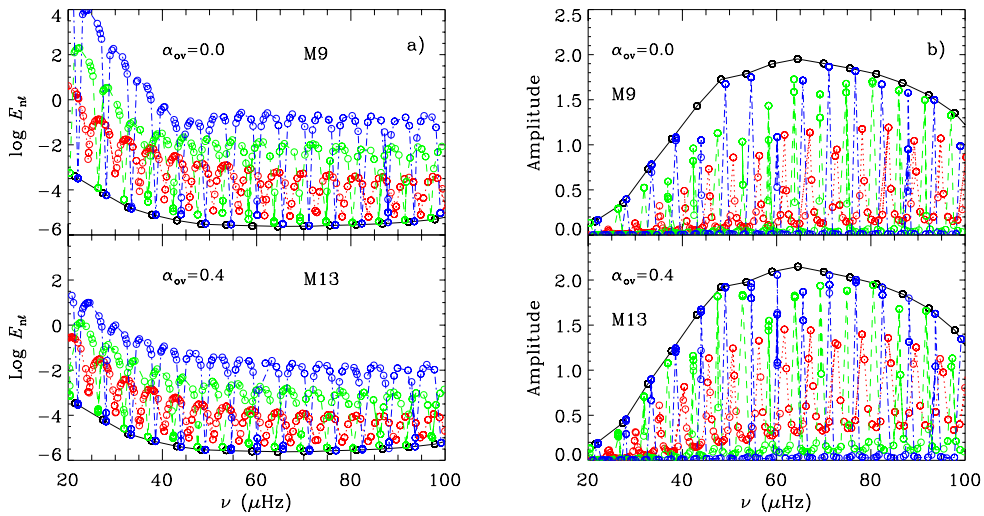

Fig. 5 (a) Mode inertias in units of $3MR^3$, plotted against frequency, for the models M09 and M13, for $\ell = 0$ (open circles connected by a solid line in black), $\ell = 1$ (open circles connected by a dotted line in red), $\ell = 2$ (open circles connected by a dashed line in green), and $\ell = 3$ (open circles connected by a dot-dashed line in blue). (b) Predicted theoretical amplitudes $\sim E_{\rm mode}^{-1/2}$. The same line styles are used as in panel (a).

there are more modes which minima in $E_{n\ell}$ which almost coincide with the radial modes, therefore, more solar-like oscillatory behaviors appear. Modes having inertia with $\alpha_{\rm ov} = 0.4$ decrease by a factor of two or three. For low-degree modes, the different behaviors of inertia in the cases with and without overshooting are a consequence of the different depths of the convection zones.

Given the mode inertia, Figure 5(c) shows that the mode amplitudes change significantly with overshooting, which could be approximately obtained by using Equation (8), normalized to unit amplitude for radial modes. From Figure 5(c), we see that the amplitude of the $\ell = 1$ modes increases with the inclusion of overshooting, but it is lower than that of the $\ell = 2, 3$ modes. It is likely that the $\ell = 1$ modes are excited in the deeper interior of the star, and hence are more strongly damped than the $\ell = 2, 3$ modes. For the $\ell = 2, 3$ modes trapped in the envelope, the inertias are close radial modes, therefore, they are characterized by substantial amplitudes compared to acoustic modes. In particular, comparing M9 with M13, we see that the average amplitudes of the $\ell = 2, 3$ modes without overshooting are obviously lower than those of the modes with overshooting because of larger inertia. For the mode trapped in the envelope, because excitation and damping occur in the upper part of the convective envelope, the variation of the modes' inertia due to overshooting can significantly affect the amplitude in terms of its magnitude and detectability. As a result, non-radial modes with overshooting might be more easily excited to observable amplitudes in red giant stars.

4 DISCUSSION

In this work, we have attempted to investigate the influence of convective core overshooting on stellar structure and pulsation properties. In Section 3, we have seen that the size of an external convective zone decreases with the increases in overshooting. The changing chemical composition results in a strong enhancement of N^2, and the sharpness of the gradient of the sound speed c at its frontier.

Due to ε Oph's advanced evolutionary stage and strong mode mixing, no regular spacing can be seen for the $\ell = 1$ modes and some of the $\ell = 2$ modes. Comparing models with and without overshooting, we found that increasing convective core overshooting decreases mode inertia, but increases mode amplitude. Thus, the $\ell = 1, 2$ modes with overshooting might be more easily observed than those without overshooting. It is clear that only more accurate observation will allow investigation of stellar properties of the interior and discrimination among the several possible evolutionary models. The combined red giant model and asteroseismic investigation would be an important step to help us give strong constraints on the stellar parameters and core overshooting.

Acknowledgements This work was supported by the Ministry of Science and Technology of the People's Republic of China (Grant No. 2007CB815406), and by the National Natural Science Foundation of China (Grant Nos. 10773003, 10933002 and 10778601).

References

Asplund, M., Grevesse, N., Sauval, A. J., et al. 2005, A&A, 431, 693
Audard, N., Provost, J., & Christensen-Dalsgaard, J. 1995, A&A, 297, 427
Barban, C., Matthews, J. M., de Ridder, J., et al. 2007, A&A, 468, 1033
Basu, S., & Antia, H. M. 2008, Phys. Rep., 457, 217
Bi, S. L., Basu, S., & Li, L. H. 2008, ApJ, 673, 1093
Cayrel de Strobel, G., Soubiran, C., & Ralite, N. 2001, A&A, 373, 159
Christensen-Dalsgaard, J. 2004, Sol. Phys., 220, 137
Cunha, K., Hubeny, I., & Lanz, T. 2006, ApJ, 647, L143
De Ridder, J., Barban, C., Carrier, F., et al. 2006, A&A, 448, 689
De Ridder, J., Barban, C., Baudin, F., et al. 2009, Nature, 459, 398
Di Mauro, M. P., Christensen-Dalgaard, J., Kieldsen, H., et al. 2003, A&A, 404, 341
Dupret, M.-A., Belkacem, K., Samadi, R., et al. 2009, A&A, 506, 57
Ferguson, J. W., Alexander, D. R., Allard, F., et al. 2005, ApJ, 623, 585
Frandsen, S., Carrier, F., Aerts, C., et al. 2002, A&A, 394, L5
Gough, D. O. 1984, Mem. Soc. Astron. Ital., 55, 13
Guenther, D. B., Demarque, P., Kim, Y.-C., & Pinsonneault, M. H. 1992, ApJ, 387, 372
Guenther, D. B. 1994, ApJ, 422, 400
Hekker, S., Aerts, C., de Ridder, J., & Carrier, F. 2006, A&A, 458, 931
Hekker, S., Kallinger, T., Baudin, F., et al. 2009, A&A, 506, 465
Iglesias, C. A., & Rogers, F. J. 1996, ApJ, 464, 943
Kallinger, T., Guenther, D. B., Matthews, J. M., et al. 2008, A&A, 478,497
Kallinger, T., Weiss, W. W., De Ridder, J., et al. 2009, ASPC, 404, 307
Mazumdar, A., Mérand, A., Demarque, P., et al. 2009, A&A, 503, 521
Richichi, A., Percheron, I., & Khristoforova, M. 2005, A&A, 431, 773
Rogers, F. J., & Nayfonov, A. 2002, ApJ, 576, 1064
Tassoul, M. 1980, ApJS, 43, 469
Unno,W., Osaki, Y., Ando, H., et al. 1989, Nonradial Oscillations of Stars (2nd ed., Tokyo: University of Tokyo Press)